Available online at www.sciencedirect.com

ScienceDirect

Polar Science 8 (2014) 96–113

http://ees.elsevier.com/polar/

Geocryological characteristics of the upper permafrost in a tundra-forest transition of the Indigirka River Valley, Russia

Go Iwahana [a,b,e,*], Shinya Takano [b], Roman E. Petrov [c,e], Shunsuke Tei [b], Ryo Shingubara [b], Trofim C. Maximov [c,e], Alexander N. Fedorov [d,e], Alexey R. Desyatkin [c], Anatoly N. Nikolaev [d,e], Roman V. Desyatkin [c], Atsuko Sugimoto [b]

[a] *International Arctic Research Center, University of Alaska Fairbanks, AK, USA*
[b] *Faculty of Environmental Earth Science, Hokkaido University, Sapporo, Japan*
[c] *Institute for Biological Problems of Cryolithozone, Siberian Branch of the Russian Academy of Sciences, Yakutsk, Sakha, Russia*
[d] *Melnikov Permafrost Institute, Siberian Branch of the Russian Academy of Sciences, Yakutsk, Sakha, Russia*
[e] *North-Eastern Federal University in Yakutsk, Yakutsk, Sakha, Russia*

Received 26 April 2013; revised 17 January 2014; accepted 24 January 2014
Available online 5 March 2014

Abstract

Understanding geocryological characteristics of frozen sediment, such as cryostratigraphy, ice content, and stable isotope ratio of ground ice, is essential to predicting consequences of projected permafrost thaw in response to global warming. These characteristics determine thermokarst extent and controls hydrological regime—and hence vegetation growth—especially in areas of high latitude; it also yields knowledge about the history of changes in the hydrological regime. To obtain these fundamental data, we sampled and analyzed unfrozen and frozen surficial sediments from 18 boreholes down to 1–2.3 m depth at five sites near Chokurdakh, Russia. Profiles of volumetric ice content in upper permafrost excluding wedge ice volume showed large variation, ranging from 40 to 96%, with an average of 75%. This large amount of ground ice was in the form of ice lenses or veins forming well-developed cryostructures, mainly due to freezing of frost-susceptible sediment under water-saturated condition. Our analysis of geocryological characteristics in frozen ground including ice content, cryostratigraphy, soil mechanical characteristics, organic matter content and components, and water stable isotope ratio provided information to reconstruct terrestrial paleo-environments and to estimate the influence of recent maximum thaw depth, microtopography, and flooding upon permafrost development in permafrost regions of NE Russia.

Keywords: Ground ice; Permafrost; Indigirka; Siberia; Stable isotope; Chokurdakh

1. Introduction

The Arctic tundra ecosystem is expected to undergo rapid and significant changes, as amplified climate change and the anticipated permafrost thaw potentially

* Corresponding author. International Arctic Research Center, University of Alaska Fairbanks, AK 99775-7340, USA. Tel.: +1 9074742444.
E-mail address: giwahana@alaska.edu (G. Iwahana).

http://dx.doi.org/10.1016/j.polar.2014.01.005
1873-9652/

alter its landscape entirely. The increase in average surface air temperature in the Arctic is expected to be nearly double the global average, with precipitation to increase as well (IPCC, 2007). Warming of permafrost has been reported in Siberia (Romanovsky et al., 2007, 2010), Alaska (Osterkamp, 2005) and Canada (Smith et al., 2012) over the last several decades. Additionally, numerical models project substantial permafrost degradation during the 21st century (Koven et al., 2011; Lawrence et al., 2012), a loss that will be accentuated by rapid sea ice loss (Lawrence et al., 2008). Permafrost degradation implies the mobilization of not only a huge amount of currently confined soil organic carbon, but also a certain extent of water previously preserved as ground ice (Ping et al., 2011). The landscape change associated with permafrost thaw largely depends on ice content of the permafrost; thawing of ice-rich permafrost leads to thermokarst.

Thermokarst development in ice-rich permafrost regions is a natural hazard, and causes irreversible geomorphological changes (Haeberli and Burn, 2002). Thermokarst is the process by which characteristic landforms result from the thawing of ice-rich permafrost or the melting of massive ice (Everdingen, 1998). The formation of large depressions in the ground surface produced by thermokarst processes results in lakes or swamps, and is frequently observed in continuous permafrost zone, including Northeastern Siberia. Extremely ice-rich syngenetic permafrost, known as Yedoma, which is strongly affected by thermokarst processes, is often found in various permafrost regions. Yedoma is a Pleistocene organic-rich silty deposit, containing excessive amounts of ground ice (50–90% in volume) including huge ice wedges (Kanevskiy et al., 2011; Schirrmeister et al., 2011, 2013). Since Yedoma is distributed in a large part of permafrost regions (NE Russia, NW Alaska, central Yukon, and area across the Bering Strait referred as "Beringia"), the impacts of Yedoma thaw or erosion on related ecosystems—including rivers, estuaries, deltas, and seas—are widespread. Zimov et al. (1997) and Walter et al. (2006) concluded that the thawing of Yedoma may release a significant amount of methane (~3.8 Tg/yr), leading to further climate warming. Therefore, the feedbacks from permafrost degradation to ecological, geomorphological, and hydrological processes have been of great scientific and social concern, and the need for elucidation of its role in the ecosystem and global climate system are emphasized by many authors (Schuur et al., 2008; Francis et al., 2009; Jorgenson et al., 2010; Rowland et al., 2010; Grosse et al., 2011).

Changes in the hydrological processes and geochemistry of aquatic systems due to thawing permafrost have been examined and reported by recent studies. Shiklomanov and Lammers (2009), for example, concluded that more intensive permafrost thawing was one of the possible causes for the 2007 record Eurasian pan-Arctic river discharge into the Arctic Ocean. Thawing of organic-rich and ice-rich sediments results in the increased flow of organic matter and water into adjacent seas and rivers, promptly changing the surrounding topography and aquatic ecosystems. Attempts to determine permafrost change from geochemical analysis of river water (Bagard et al., 2011) or streamflow characteristics (Brutsaert and Hiyama, 2012; Sjoberg et al., 2013) have been conducted and have demonstrated implications of permafrost degradation. Although spatial and temporal distribution and geocryological properties of ice-rich/organic-rich permafrost have critical importance in these studies, these characteristics remain insufficiently understood. Several studies focusing on the quantification of volumetric ground ice content in tundra regions have been conducted in Arctic Alaska (e.g., Pullman et al., 2007; Kanevskiy et al., 2013), Canada (e.g., Morse et al., 2009), and Siberia (e.g., Grave and Turbina, 1980; Ershov, 1989; Strauss et al., 2012); however, the remoteness of sites, insufficient resources for frozen ground coring, and time-consuming analyses of volumetric measurements of frozen samples keep field evidence in other permafrost regions scarce.

On the other hand, geocryological characteristics such as cryostratigraphy and stable isotope ratio of cryostructure ice or ice wedges provide some information about freezing conditions and the paleoclimatic conditions under which stratigraphic parts were formed (e.g., Arkhangelov et al., 1986; Vaikmae, 1989; Michel, 2011; Mackay, 1983). The stable isotope ratio of ground ice have been intensively studied with high sampling resolution, primarily regarding ice wedges and other types of massive ground ice, in order to reconstruct mean winter temperature for the period when the ice wedges formed (e.g. Meyer et al., 2010; Opel et al., 2011). Although similar investigations regarding cryostructure ice have rarely occurred, together with the information obtained from massive ground ice, the spatial distribution of stable isotope ratio of cryostructure ice has a potential to provide important clues for the reconstruction of past environments. In addition to the geocryological information archiving the paleo-environment, the isotope ratio of near-surface permafrost that is anticipated to thaw in

the future provides essential geochemical characteristics about one of the water sources discharging to Arctic rivers. Furthermore, stable isotope ratios provide basic information to determine the source water for microbiological processes, such as methane production in thermokarst environments (Brosius et al., 2012).

Accordingly, there is a strong demand for obtaining geocryological field data, in order to reduce uncertainty surrounding the amount of ground ice and organic carbon currently stored in a frozen state and vulnerable to release upon permafrost thaw. Our objectives are to describe the current thermal regime of the active layer (seasonally thawing and freezing ground layer) and geocryological characteristics in the near-surface ground to a depth of up to 2.3 m, to capture features of spatial variation of ground ice contents and isotopes, and to interpret the diversity of the near-surface geocryology and history of development or degradation of the permafrost in the lower Indigirka River Valley.

2. Site description

Our research area is located near Chokurdakh (70° 37′ N, 147° 54′ E) in Northeastern Siberia, Russia, about 150 km inland from the Arctic sea coast along the Indigirka River (Fig. 1). In the research area, floodplain lower than 50 m a.s.l. is widespread from the Indigirka River bank toward inland about 5–20 km. Zaitsev (1989) introduced this floodplain as a Holocene deposit, and the age of near-surface sediments from this floodplain are considered in our study to be late Holocene. Remnants of Yedoma ice-complex deposits are occasionally present as various-sized hills several-tens m higher than surrounding floodplains. Outcrops of Yedoma were observed along some river banks, exposing ice wedges with widths of several-meters. Numerous thermokarst lakes, drained lake basins, and ice wedge polygons were often observed in the lower watershed. The thickness of continuous permafrost in this area is 400–700 m. Average active layer thickness ranges 0.4–0.6 m on hills, 0.4–0.8 m in northern Taiga, 0.3–0.8 m in alas (a large depression of the ground surface produced by thermokarst) complex, and 0.4–1.0 m in floodplains (Permafrost-Landscape map of Yakutskaya Autonomous Soviet Socialist Republic, 1991).

According to the Agricultural Atlas of Yakutskaya Autonomous Soviet Socialist Republic (1989), land cover type in the northern part of our research area, near the Indigirka River, is tundra-wetland with ice wedge polygons in the "river valley and maritime vegetation" category, whose vegetation includes alders (*Duschekia fruticosa*), willows (*Salix pulchra, Salix glauca*), cottongrasses (*Eriophorum vaginatum*), and sedges (*Carex stans*). Vegetation in the southern part of the research area is classified as "river valley vegetation with larch trees (*Larix gmelinii, Larix cajanderi*)," whose forest floor consists of tundra-wetland with mosses (*Aulacomnium turgidum*, *Hylocomium splendens*, *Sphagnum balticum*, etc.). Profiles upon Yedoma remnants or hills composed of Pre-Quaternary deposits or bedrocks in the research area,

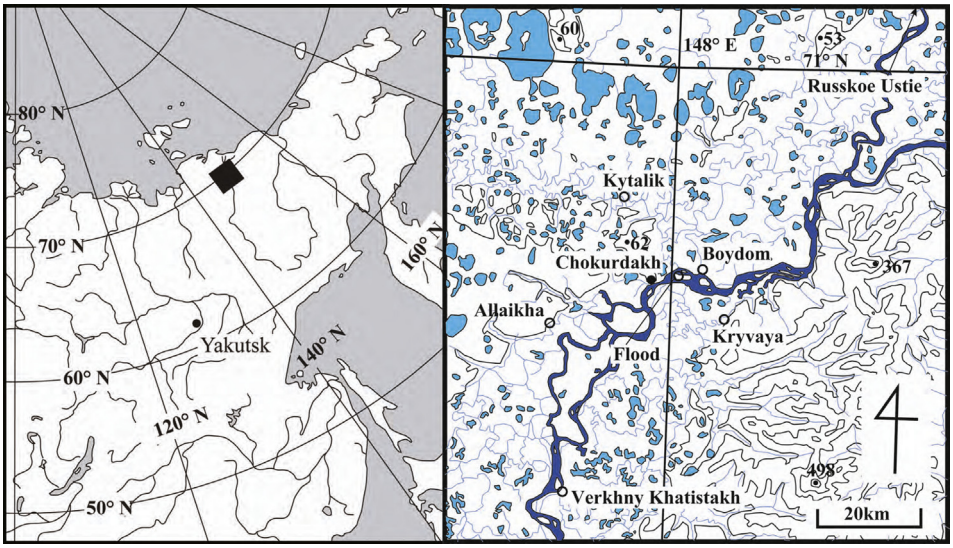

Fig. 1. Location of study sites.

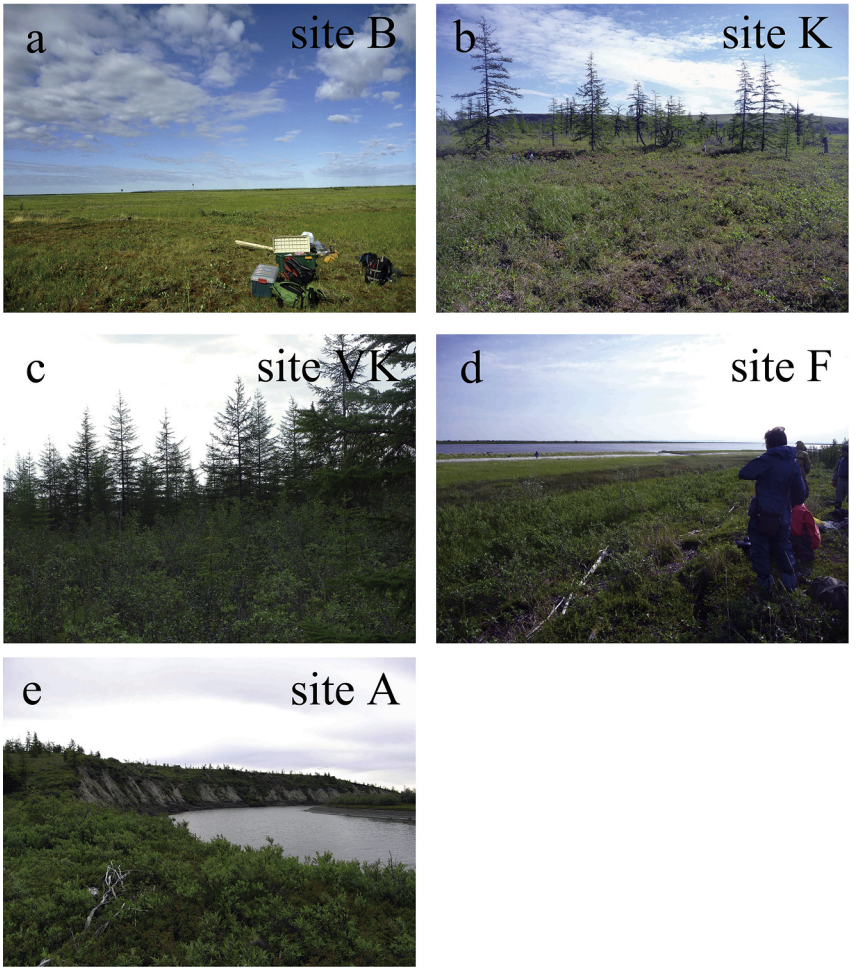

Fig. 2. Landscape of study sites.

often classified as "southern subarctic tundra," consisted of sparse shrubs (*Betula exilis*, *Salix pulchra*) with mosses and lichens (*Aulacomnium turgidum*, *Cetraria cucullata*), bushes (*Vaccinium vitis-idaea*, *Vaccinium. uliginosum*, *Ledum palustre*) with mosses (*Aulacomnium turgidum*, *Hylocomium splendens var. alaskanum*, *Cetraria cucullata*), tussock tundra, and tundra-wetland.

Based on data between 1999 and 2006 from the Chokurdakh weather station (WMO station ID 21946) and a micrometeorological flux site located in the World Wildlife Fund Kytalyk reserve 28 km northwest of Chokurdakh, Van Der Molen et al. (2007) summarized the general climatology of this area as follows: mean January, annual, and July surface air temperatures were −34.2, −10.5, and 10.4 °C, respectively. Monthly mean temperatures are quite variable in the winter and more constant in the summer. Annual mean precipitation amounts to 212 mm, of which about half falls as snow.

Five study sites were selected for soil sampling and/or ground monitoring: Boydom (Site B) is the northernmost tundra site among our study sites along the Indigirka River, Kryvaya (Site K) is situated in a forest-tundra landscape 8 km south of Site B, Flood (Site F) is on a small island in the Indigirka River, Allaikha (Site A) was chosen on the slope of a hill, and Verkhny Khatistakh (Site VK) is a larch-dominated forest near a northern end of tree line (Figs. 1 and 2). Descriptions of study sites and sampling points are summarized in Table 1. Further details about each study site follow:

Site B (Fig. 2a) is wetland tundra in the floodplain with sedges, mosses, lichens, and dwarf shrubs. Recognizable low-centered polygons with approximate diameters of 7–10 m covered most of the site, and

Table 1
Summary of study site descriptions.

Site	Latitude	Longitude	Height (a.s.l.)	Land cover type	Landscape/microtopography	Sampling point	Thaw depth (cm)	Categorization of sampling points
Boydom (B)	70°38′15″N	148°09′17″E	9 m	Tundra	Low-centered polygon	B_1	28	Dry area
						B_2	35	Wet area
						B_3	24	Wet are (polygon trough)
						B_4	14	Dry area
						B_5	25	Wet area (polygon center)
						B_6	20	Dry area
Kryvaya (K)	70°33′48″N	148°15′51″E	9 m	Forest Tundra (Boundary)	Tussock wetland/shrubs/sparse larch trees	K_1	20	Dry area
						K_2	36	Wet area
						K_3	40	Dry area
						K_4	28	Wet area
Flood (F)	70°38′09″N	148°02′53″E	6 m	Grassy plain/shrub tundra	Small island in the river	F_1	63	Upper bank
						F_2	85	Lower bank
Allaikha (A)	70°30′56″N	147°18′15″E	9 m	Shrub tundra	Yedoma remnant hill with sparse larch trees and shrubs	A_1	36	Slope of Yedoma hill
Verkhny Khatistakh (VK)	70°15′07″N	147°28′08″E	8 m	Forest	Gentle slope with larch forest and tussock wetland	VK_1	39	Lower (tussock wetland)
						VK_2	33	Middle
						VK_3	32	Higher
						VK_4	35	Lower (tussock wetland)
						VK_5	33	Higher

several small larch trees (<3 m) stood on relatively higher and dryer areas (Dry area). Ground monitoring has been conducted at the Dry area. Soil core samples were taken at six points: the ground monitoring point (Dry area), another two Dry area points, in the middle of a low-centered polygon (Wet area), and two points on rims of the polygon (Wet area). Thaw depths were obtained only at the core sampling points; 14 cm (Dry area)/20 cm (Dry area)/25 cm (Wet area) on 21 July 2009 and 28 cm (Dry area)/24 cm (Wet area)/35 cm (Wet area) on 14 July 2010.

Site K (Fig. 2b) is forest tundra in the floodplain situated on a transition zone of tundra and forest along the Indigirka River. Small larch trees (<3 m) were sparsely distributed at patchy, relatively higher and dryer areas. Other vegetation and landscapes were similar to site B, except for apparent polygonal features on the surface. A small wetland area (<20 m in diameter) sporadically covered this site. Ground monitoring has been conducted at a dry area. Soil core samplings were made at the ground monitoring point, another two points at relatively higher and dryer areas, and at two wetland area points. The spatial averages of thaw depths on 22 July 2009 were 0.32 m ($n = 20$) at dry areas and 0.37 m ($n = 20$) at wetlands, respectively.

Site VK (Fig. 2c), the Verkhny Khatistakh site, is a dense forest in the floodplain consisting of larch, willows, and alders. The approximate height of the forest crown was up to 10 m. The forest was located on generally flat ground about 50 m inland from the river bank. Relatively low area of the site became less dense with trees, and wetlands with tussocks and mosses covered some areas. We set five points for core sampling along a gentle slope transect in the forest (less than 0.02% slope)—two points at higher and dryer areas of the forest, two points between tussocks in the wetland, and one at the middle of the slant for core sampling. The ground monitoring sensors were installed at the higher area of the forest. The spatial average of thaw depths on 23 July 2009 were 0.28 m ($n = 20$) in the forest and 0.44 m ($n = 20$) at the wetland, respectively.

Site F (Fig. 2d) was formed by two levels of floodplain terraces. The lower river bank was partly covered by herbaceous plants or graminoids, and was obviously a frequently or seasonally flooding area. A terrace with low Salix sp., about 1.5 m higher than the lower bank, occurred about 80 m inland from the river. We sampled 1.5 m cores at each terrace level. Thaw depths averaged about 0.60 m ($n = 9$) and 0.80 m

($n = 32$) on 21 July 2010 on the higher terrace and the river bank, respectively.

Site A (Fig. 2e) is on a slope of a hill with the maximum height of more than 50 m. Soils were sampled at a single slope point at an approximate height of 25 m a.s.l., which represents the highest sampling point in this study. The spatial average of thaw depth was 0.35 m ($n = 20$) on 24 July 2009, on the slope of the hill.

3. Methods

The measurement period for ground and meteorological monitoring presented in this paper is from July 2009 to September 2011. Data obtained included gaps because of malfunctions of sensors or loggers and disturbance by animals. In this study, the physical ground surface was used as a zero depth.

3.1. Ground and meteorological measurements

Air temperature data were obtained from the Chokurdakh weather station (WMO station ID 21946). Precipitation data were provided from the Kytalyk micrometeorological flux site (personal communication; Van Der Molen et al., 2007). Ground temperature (0.01, 0.05, 0.1, 0.2, 0.3, 0.4, 0.5, 0.75, and 1.0 m below the ground surface) and air temperature (0.1, 0.2, 0.3, and 0.4 m above the surface) were measured with thermistor sensors (TMC-HD; Onset Computer Co.). Volumetric water content was measured with EC-5 or EC-20 sensors (Decagon Devices, Inc.). Ground measurement data were recorded by data loggers (HOBO U12-006; Onset Computer Co.). Seasonal change in snow depth at the VK site was estimated roughly from fluctuations in air temperature at various heights, assuming air temperature at the height under the snow surface was recorded with significantly lower standard deviation than air at above the snow surface.

3.2. Soil and water sampling

Soil cores down to 3-m depth were sampled in July 2009 and 2010 using a power auger (Tanaka TIA-350S), with core samples of φ2–3 inches (5–7.6 cm). Sampled cores were cleaned to remove contaminations, cut to 2–15 cm long, wrapped with polyethylene stretch film, and double sealed with polyethylene packs. Lengths and circumference of columnar cores were measured in the field to calculate the volume of the samples. Frozen samples were then thawed in the sealed packs, and supernatant water was stored in vial bottles for isotope analyses. Water was extracted using centrifuge from samples containing inadequate amounts of water. River water was sampled during transportation between sites from motor boats.

3.3. Water stable isotope

The isotopic compositions of water (hydrogen and oxygen) were analyzed by the $CO_2/H_2/H_2O$ equilibration method using a Delta V (Thermo Fisher Scientific, USA, manufactured in Germany) attached to a Gas Bench (Thermo Fisher Scientific, USA) at Hokkaido University, Japan (Ueta et al., 2013). These data were expressed as δD or $\delta^{18}O$ values, defined as δ_{Sample} (‰) $= (R_{Sample}/R_{VSMOW} - 1) \times 1000$, where R is the isotope ratio of water (D/H or $^{18}O/^{16}O$), and subscripts Sample and VSMOW refer to samples and standard (i.e. Vienna Standard Mean Ocean Water), respectively. The analytical errors for the whole procedure were within 2% and 0.2% for δD and $\delta^{18}O$, respectively. Deuterium excess (d-excess) was calculated as d-excess $= \delta D - 8 \times \delta^{18}O$ (Dansgaard, 1964), which is an indicator of non-equilibrium processes such as evaporation (e.g., Merlivat and Jouzel, 1979).

3.4. Soil analysis

Selected soil samples were well mixed, and gravimetric organic matter content was roughly estimated by loss on ignition (LOI) at 500 °C (e.g. Heiri et al., 2001). The grain size distribution of the sampled soils was determined by the Kachinsky method (1958), and their texture was arbitrary classified based on the USDA Texture Diagram (Soil Survey Staff, 1999). Cryostructures of frozen samples were classified based on Murton and French (1994).

4. Results and interpretation

4.1. Air temperature and ground thermal conditions

During the summers of 2010 and 2011, the research area had experienced significantly warmer temperatures after a summer in 2009 that was cooler than the long-term norm (Fig. 3). Monthly mean air temperature in the warmest month (July) of 2009 was 8.6 °C. In July 2010 and 2011, equivalent values were 17.4 and 14.0 °C, respectively, which were anomalously higher than the recent long-term average (10.4 °C). Winter temperature before the three thawing seasons was close to the recent norm condition. Monthly mean air

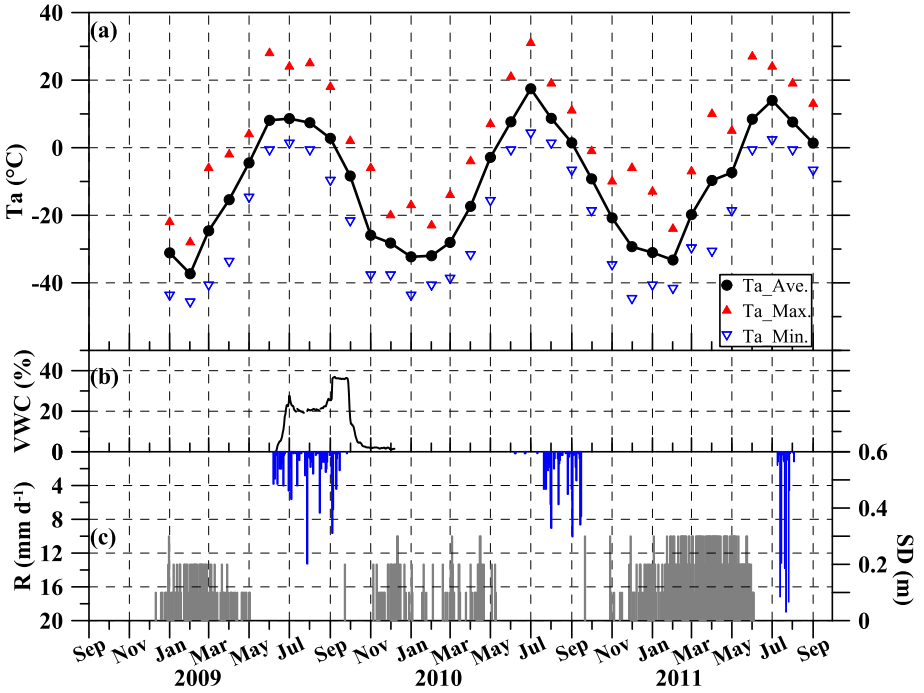

Fig. 3. Meteorological records during study period: (a) Ta, VWC, R, and SD indicate air temperature, (b) volumetric soil water content at 5 cm depth of site B, (c) rainfall, and snow depth, respectively. Monthly mean (Ta_Ave.), maximum (Ta_Max.), and minimum (Ta_Min.) air temperatures are shown in (a).

temperatures in the coldest month (February in 2009 and 2011 and January in 2010) were −37.3, −32.3, and −33.2 °C, respectively (the long-term average is −34.2 °C). Monthly mean soil temperatures at 0.5-m depth were −0.2, −0.3, and −0.1 °C in September 2009, at respective sites B, K, and VK. In September 2010, these numbers increased respectively to 0.1, 0.3, and 0.2 °C affected by warmer summer.

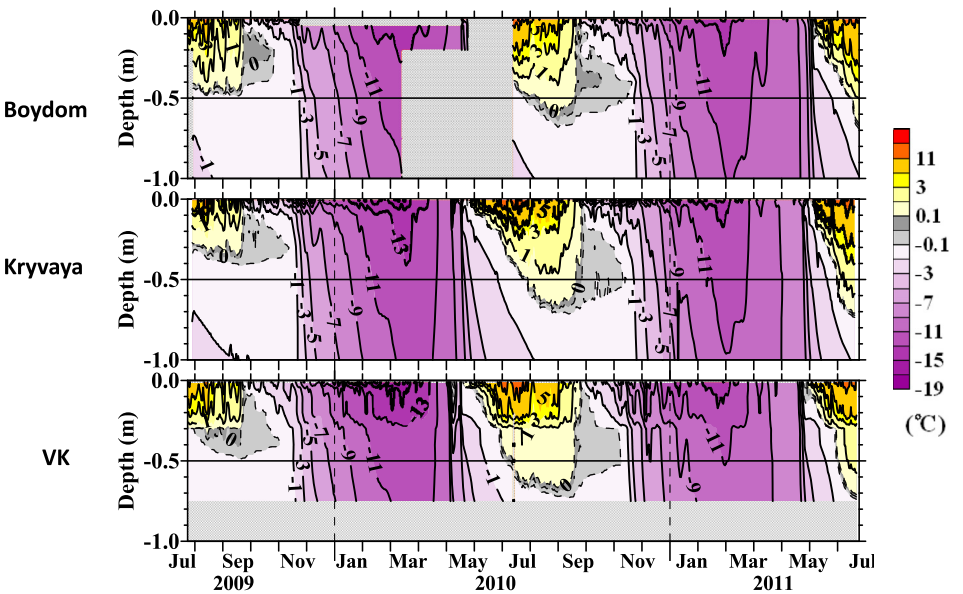

Fig. 4. Seasonal change in ground temperature profiles at sites B (Boydom), K (Kryvaya), and VK from July 2009 to July 2011 based on daily mean measurements. Solid isotherms are drawn with increments of 2 °C, and the dashed lines indicate the ±1 and 0 °C isotherms.

The general trends in ground thaws at three monitoring points are as follows (Fig. 4): Ground thaw began at the latter half of May, following by stable progress of thaw front. Thawing rate, for example, at site K during June–July in 2010 was 0.9 cm/day. Maximum thaws were observed at the end of August or beginning of September. The closure of the zero curtain (Outcalt et al., 1990) was completed by the middle of November. Winter penetration of cold temperature at site VK and the summer thawing rate are relatively moderate compared to other tundra sites. Other marked differences in ground thermal regime and maximum thaw depths between monitoring sites was subtle; however, the differences in maximum thaw depth were remarkable between years. The maximum thaw depths in 2010 and 2011 were 0.65–0.72 and 0.70–0.72 m, respectively, and 0.40–0.49 m in 2009. This large annual difference in active layer thickness can be attributed partly to the consecutive anomalously warm summers in 2010 and 2011, and partly to winter surface conditions such as changes in snow depth and air temperature. Snow depth as a controlling factor of ground temperature in permafrost regions has been emphasized by numerous studies (e.g. Palmer et al., 2012).

4.2. Soil grain size and frost susceptibility

Characteristics of soil grain size distribution at study sites demonstrated dependence on the locations of the sites within the floodplain. Sites close to the main stream of the Indigirka River tended to contain coarser soil, and soils at sites further from the main stream or along secondary streams tended to have finer particles (Figs. 6, 8, 10 and 12). For example, site F stands in a landmass near the main stream and site VK along the mainstream, and their soils contained significantly larger proportion of sand than the soils at site K, which was the farthest from the mainstream. F1 soils contained a large portion of sand and classified as silt loam or sandy loam. VK3 soils varied between loam and clay loam in the profile. B1 soils were loam or silt loam with small variation along depth. K3 soils gradually changed from silty clay loam to clay loam upward. Inclusion of gravels was rare. Although we were able to conduct grain size analysis for a limited number of samples, all soil samples analyzed were classified as frost-susceptible, based on the finer percentage curve (e.g. Casagrande, 1932; Beskow, 1935). Under the same effective stress, frost heave ratio (ratio of total heave length to initial soil length) is inversely proportional to freezing speed (Takashi et al., 1974). Together with a prolonged small temperature gradient (zero curtain) at the beginning of winter (which produced slow freeze back from both the top and bottom of the active layer), abundant soil water in wetlands, frost susceptible soils, and the formation of ice lenses made the near-surface ground of the studied areas excessively ice-rich.

4.3. Ice content, organic matter content, stable isotope ratio, and cryostratigraphy

Site B (Figs. 5 and 6)

Most samples contained excess ice (supernatant water appeared upon thaw) due to inclusion of numerous ice lenses with various thickness; volumetric ice content was around 60–95%, showing large variation with depth down to 1.5 m. Little relationship exists between ice lens thickness and volumetric ice content. Numerous vertically elongated air bubbles were often observed within thick ice lenses. Several samples from dry areas (B1, B4, and B6) were unsaturated with water, probably because of desiccation

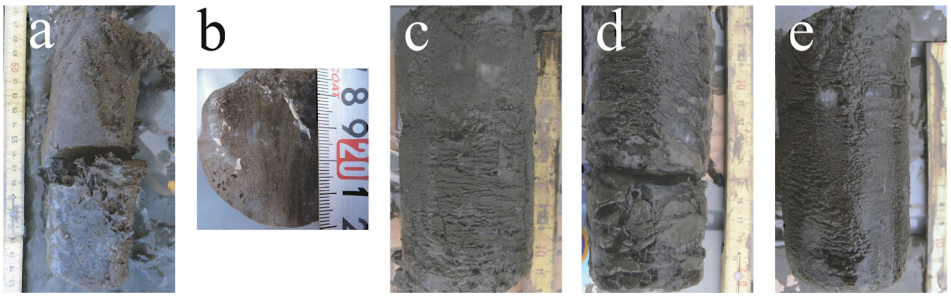

Fig. 5. Examples of cryostratigraphic features in frozen core samples from site B: (a) peat or plant residues (B2 depth 0.47–0.65 m); (b) wedge ice (B3 depth 1.00 m); (c) structureless (upper part) and wavy non-parallel layered or lenticular cryostructures, with fine and thin ice lenses (lower part) (B4 depth 0.54–0.63 m); (d) suspended cryostructure with moderate to thick ice lenses or inclined ice veins (B4 depth 0.69–0.83 m); (e) wavy non-parallel layered, lenticular, or transitional to suspended cryostructures with thin and moderate ice lenses (B4 depth 0.90–1.00 m). Photo scales are in centimeters.

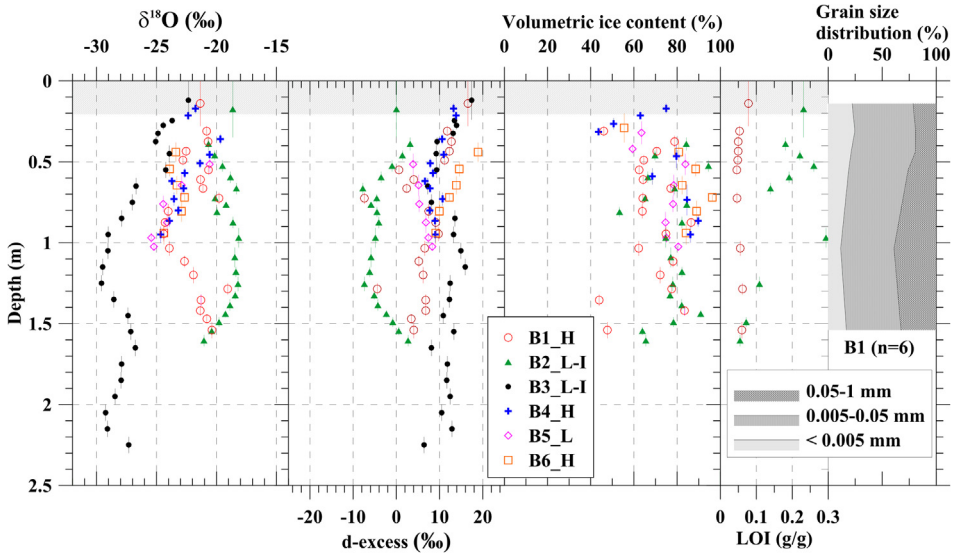

Fig. 6. Profiles of oxygen stable isotope ratio, d-excess, volumetric water content, loss on ignition, and grain size distribution at site B. The letters H, L, and I with sampling locations indicate higher dry areas, lower wet areas, and ice wedge, respectively. Hatched area in the upper part of figure corresponds to average thaw depth at the time of sampling.

when the soil experienced differential freezing associated with ice segregation. Core samples at B2, taken from an area of low-centered polygon (wet area), included large amounts of peat or plant residues (Fig. 5a) showing high LOI (0.1–0.3 g/g). The B3 core was taken from an ice wedge of polygon troughs. B3 samples showed vertical foliation, and a countless number of air bubble inclusions were found, indicating ice wedge origins of the ground ice (Fig. 5b).

Unsaturated samples or those with low ice content had structureless cryostructure (Upper part of the core in Fig. 5c). Cryostructure of ground ice at dry areas (B1, B4, and B6) was mainly wavy non-parallel layered or lenticular (Fig. 5e) with fine (<1 mm) or thin (1–5 mm) ice lenses, but occasionally contained suspended cryostructure (Fig. 5d) with moderate (5–10 mm) to thick (>10 mm) ice lenses or inclined ice veins. Cryostructure in the B2 profile was suspended cryostructure. B5 core had similar cryostructure, but consisted mainly of thicker ice lenses and veins.

Profiles of oxygen stable isotope ratio varied the most between different types of ground ice. While ice wedge profile (B3) showed the lowest $\delta^{18}O$ values (around −28‰), the values in the peat rich profile (B2) were the highest (about −19‰) at the site. $\delta^{18}O$ values of samples at the other locations (B1, B4, B5, and B6) ranged between the values at B2 and B3. The lower $\delta^{18}O$ values at B3 can be attributed to ice wedges usually originating from snow melt water in spring (e. g., Mackay, 1983; Meyer et al., 2010). The values around −28‰ were also found, for instance, in Yedoma ice complex on Big Lyakhovsky Island, about 350 km northeast from Chokurdakh (Meyer et al., 2002). It should be noticed that the age of wedge ice sampled in this study is thought to be late Holocene, and that of the Yedoma ice in Meyer et al. (2002) late Pleistocene. The source of the ground ice at B2 was expected to be snow melt water similar to ice wedges, as B2 was located at a relatively low area and it

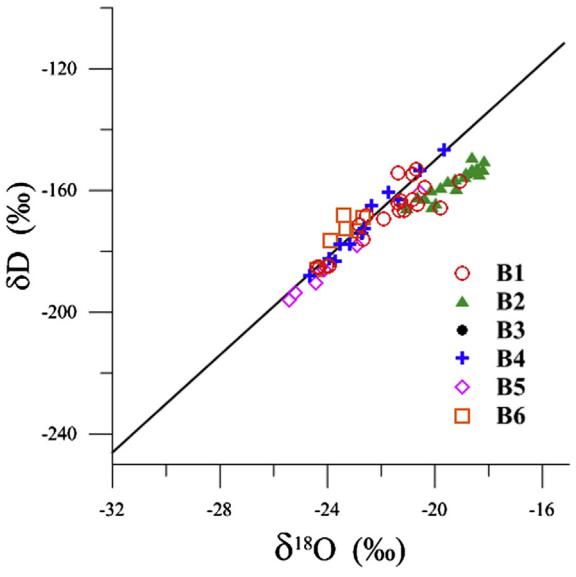

Fig. 7. Co-isotope relationship of ground water/ice at site B.

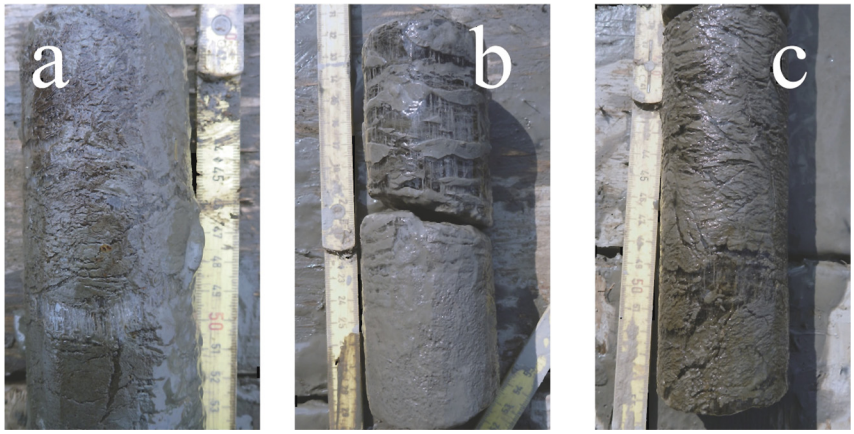

Fig. 8. Examples of cryostratigraphic features in frozen core samples from site K: (a) Organic matter-rich core with irregular lenticulate or transitional to suspended cryostructures (K1 depth 0.40–0.53 m); (b) suspended (upper part) and structureless cryostructures (lower part) (K1 depth 1.13–1.28 m); (c) irregular lenticulate or transitional to suspended cryostructures, with various thickness of ice lenses (K1 depth 1.38–1.54 m). Photo scales are in centimeters.

preferentially collected the melting water. However, stable isotope ratios at B2 and B3 distinctly differ, indicating completely different origins of their ground ice profiles. The origin of B2 water, in particular, may be attributed to rain or river water. Most d-excess values were plotted near the Global Meteoric Water Line (GMWL), while the values at B2 showed markedly deviation from the GMWL (Fig. 7). This indicates that the source water of B2 samples was influenced by evaporation (e.g., Merlivat and Jouzel, 1979).

Site K (Figs. 8 and 9)

Volumetric ice contents excluding wedge ice at site K ranged between 60 and 95%, with less variation in the values among sampling location or along depth than at site B. All frozen samples were water saturated. In the upper 1.5 m, regardless of the sampling location, cryostructure was dominated by wavy non-parallel lenticular or suspended cryostructures with occasional occurrence of structureless cryostructure (Fig. 8). The cores sometimes encountered massive

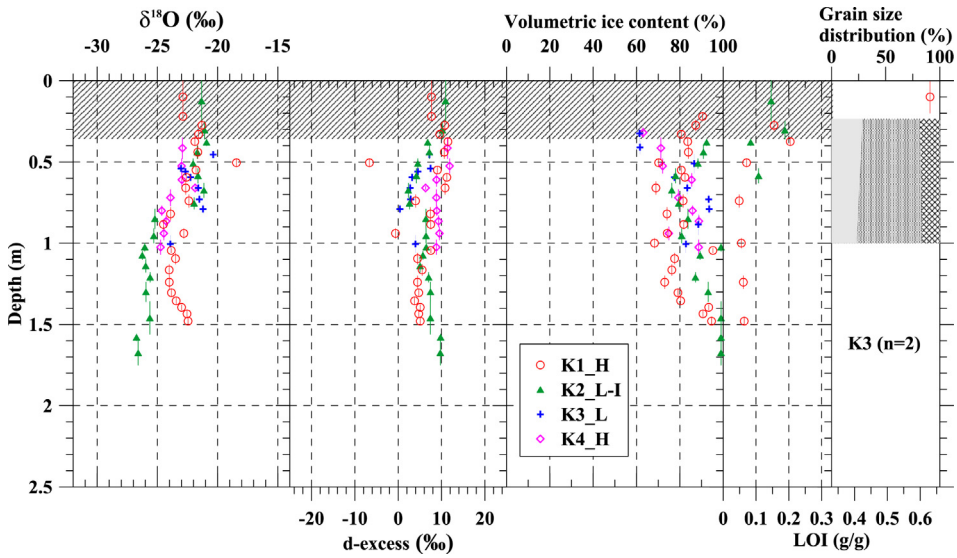

Fig. 9. Profiles of oxygen stable isotope ratio, d-excess, volumetric water content, loss on ignition, and grain size distribution at site K. The letters H, L, and I with sampling locations indicate higher dry areas, lower wet areas, and ice wedge, respectively. Legend for grain size is the same as in Fig. 6. Hatched area in the upper part of figure corresponds to average thaw depth at the moment of sampling.

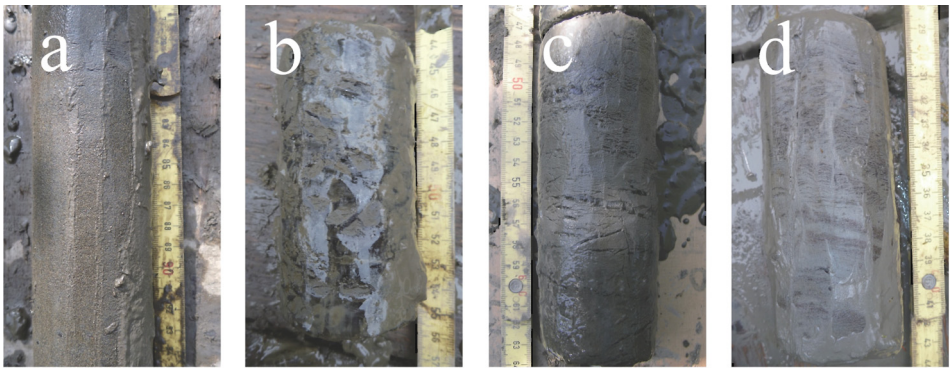

Fig. 10. Examples of cryostratigraphic features in frozen core samples from site VK: (a) structureless cryostructure (VK1 depth 0.77–0.95 m); (b) suspended cryostructure (VK3 depth 0.45–0.55 m); (c) wavy non-parallel layered or lenticular, with various thicknesses of ice lenses (VK5 depth 0.48–0.63 m); (d) brownish laminar structure with rich organic matter and wavy non-parallel layered cryostructure, with thin ice lenses (VK3 depth 1.30–1.42 m). Photo scales are in centimeters.

ice—most likely ice wedge portions—at certain depths, especially at K2. Ice with peat began at 1.0 m depth, and from 1.56 m, pure wedge ice continued. Organic matter content was particularly high among upper 0.6 m profiles (e.g. Fig. 8a).

Values of $\delta^{18}O$ seemed to decrease toward the permafrost table in the active layer, from around −22‰ to −25‰. Below 1.0 m depth, ice wedge (K2) $\delta^{18}O$ values were lowest (about −27‰), and the values at K1 showed smooth changes around −24‰. It is worthwhile to note that d-excess values in the lower active layer (0.5–0.7 m depth) at wet areas (K2 and K3) were remarkably lower than those at dry areas (K1 and K4). This lower d-excess may be explained by site-specific micro-reliefs, which determine the areas that preferably collect meteoric water (relatively low wet areas) and maintain water ponding, exposing water to evaporation during summer; somewhat similar relationship between dry areas and wet areas can be seen in d-excess at site B as well.

Site VK (Figs. 10 and 11)

Grain size distribution of the samples at site VK varied with depth and among sampling locations to a larger extent than at sites B and K. Sandy samples had

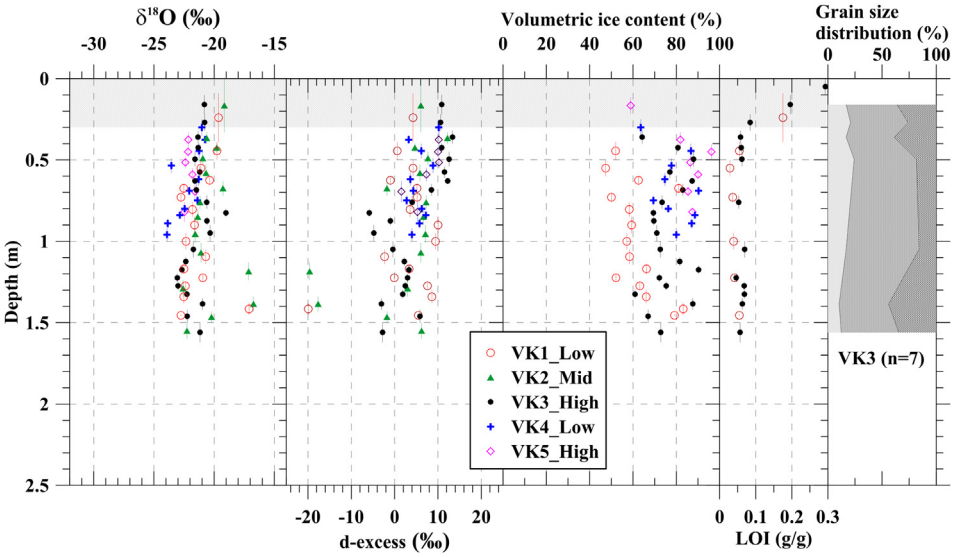

Fig. 11. Profiles of oxygen stable isotope ratio, d-excess, volumetric water content, loss on ignition, and grain size distribution at site VK. The remarks Low, Mid, and High with sampling locations indicate lower, middle and higher location on the sampling transect, respectively. Legend for grain size is the same as in Fig. 6. Hatched area in the upper part of figure corresponds to average thaw depth at the moment of sampling.

lower ice contents and structureless cryostructure (Fig. 10a), which lead to a wide range of volumetric ice content excluding wedge ice at this site (45–95%). Most of the VK1 and VK2 soil profiles, and a portion of VK3 and VK4, showed structureless or wavy non-parallel lenticular cryostructure, with fine and thin ice lenses and veins, making their ice content smaller (Fig. 10c). Thick and moderate ice lenses and veins were found exclusively at relatively higher locations (VK3 and VK5), forming wavy non-parallel lenticular or suspended cryostructure (Fig. 10 b). Plant roots were often found in the soil profile of VK4, and brownish laminar structure with rich organic matter (Fig. 10d) was found in the lower profile of VK3 (1.3–1.62 m), indicating past temporal paludification of the location.

The d-excess values in the active layer at site VK appeared to show differences similar to site K. The lower and wetter area (VK1, VK3, and VK4), where meteoric water can gather preferably, contained water affected by evaporation in their active layers. No marked feature in the profiles of $\delta^{18}O$ as a whole was found; however, it seemed that $\delta^{18}O$ and d-excess at VK3 were relatively stable with depth, while they apparently fluctuate below the active layer.

Sites F & A (Figs. 12 and 13)

In order to explore processes of the active layer and upper permafrost development in the research area, soil and ground ice analysis at two cores from a frequently flooding island in the river and at the higher Yedoma hill are compared in Fig. 13.

At site F, soils were frozen at depths of 0.63 and 0.90 m at F1 and F2, respectively. Soils in the active layer were clearly unsaturated with water. Fractions of sandy particles in these samples were largest among the study sites, and cryostructure was either poorly developed or showed wavy non-parallel layered cryostructure with fine/thin ice lenses and organic matter layers below depth in the frozen samples (Fig. 12a). Volumetric ice

Fig. 12. Examples of cryostratigraphic features in frozen core samples from sites F and A: (a) wavy non-parallel layered cryostructure with fine/thin ice lenses and organic matter layers (F2 depth 1.28–1.58 m); (b) wavy non-parallel layered or lenticular cryostructure (A depth 0.55–0.75 m). Photo scales are in centimeters.

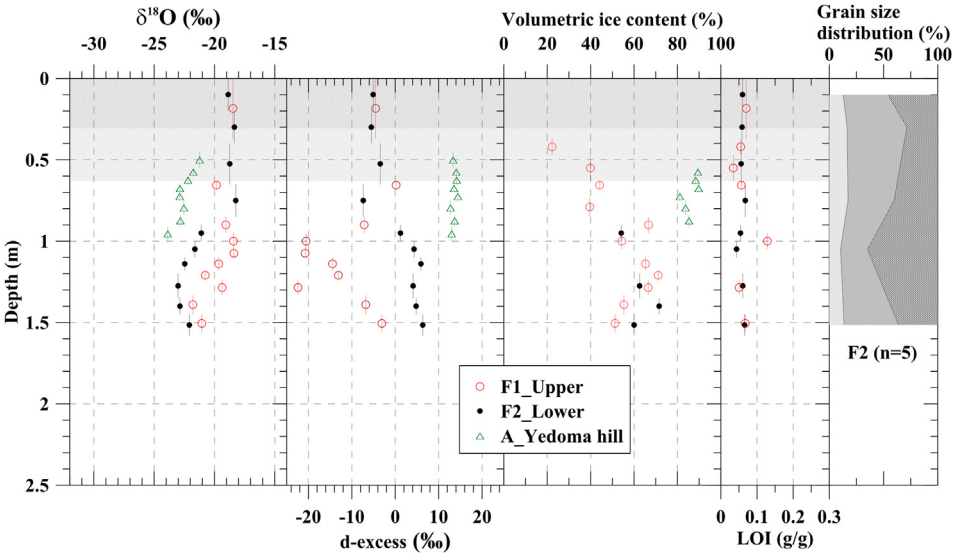

Fig. 13. Profiles of oxygen stable isotope ratio, d-excess, volumetric water content, loss on ignition, and grain size distribution at sites F and A. The labels Upper and Lower with sampling locations indicate the sampling point on the upper and the lower bank, respectively. Legend for grain size is the same as in Fig. 6. Hatched and double-hatched areas in the upper part of figure correspond to average thaw depths at the moment of sampling at sites F and A, respectively.

contents of frozen soil samples at site F were 50–70%. $\delta^{18}O$ values (around −19‰) and d-excess values (between 0 and -9‰) were similar in the upper 0.9 m soil profiles of F1 and F2 (Fig. 13). This feature in stable isotope ratio remarkably resembles those of B2. On the other hand, below depth of 0.9 m, the isotope composition of ground ice contained in frozen soils at F1 and F2 was distinctly different (Fig. 13).

Frozen soils of the upper permafrost at site A contained around 85% volumetric ice, with wavy non-parallel layered or lenticular cryostructure, which was often observed at dry areas or at higher locations at other sites (Fig. 12b). $\delta^{18}O$ values were comparable to those found in the soil profiles at dry areas in B, K, and VK sites, and d-excess values were nearly constant at around 11–12‰, indicating small influence of evaporation on isotope composition of water before it had been fixed on-site at site A. $\delta^{18}O$ values gradually decreased from −21 to −24‰.

4.4. Diversity and indications of near-surface geocryology

Geocryological characteristics of frozen ground including ice content, cryostratigraphy, soil mechanical characteristics, organic content and components, and water stable isotope ratio contain certain information about the surface environment during the permafrost formation. Studied volumetric ice contents in the frozen sediment samples varied in a wide range (40–96%). The average volumetric ice contents for pore and segregated ice of frozen samples were 74, 83, 75, 60, and 86% at B, K, VK, F, and A sites, respectively. The overall average of ice contents of the floodplain frozen samples excluding wedge ice was 75%, which is comparable to near-surface volumetric ice contents of soil (due to pore and segregated ice) at coastal plain or drained-lake basins of the Beaufort Sea coast of Alaska (around 80%) reported by Kanevskiy et al. (2013). On the other hand, the lower range of ice content (20–60%) for Holocene floodplain sediments in maritime lowlands of Yakutia was reported by Kuznetsova (1980). In our study, the ice contents and cryostructure seemed to vary depending on the soil grain size distribution, locations within each sites' microtopography, or vicinity to the river from the sites. The diversity in geocryological characteristics at the study sites can be attributed to temporal change and spatial difference in hydrological regimes caused by landscape and micro-relief. Conversely, the development of micro relief could be explained by spatial distribution of cryostructure in near-surface permafrost together with spatial variation of sedimentation. In other words, locations with higher frost-heave extent by segregated ice in permafrost may become higher and drier, allowing taller vegetation growth in floodplains. Understanding the spatial variation in geocryological conditions is important to reconstruct paleo-environment of permafrost regions; additionally, this information may be used to reconstruct past

greenhouse gas fluxes because methane fluxes, for example, are highly sensitive to hydrological conditions and vegetation composition in tundra (Van Huissteden et al., 2005; Van Der Molen et al., 2007). Further analysis with increased number of samples is required to obtain more rigorous relationship between site geography and geocryology.

In Table 2, statistics for $\delta^{18}O$, δD, and d-excess of river and soil water in the upper (0–0.5 m depth) and lower layers at study sites are summarized. A common feature for the stable isotope ratio of soil water at floodplain sites was that average values of $\delta^{18}O$ and δD from the lower soil layers (>0.5 m) was higher (0.7–1.9 and 11–15‰, respectively) than those from the upper layers. While averages of $\delta^{18}O$ and δD at floodplains showed similar values, d-excess values varied to a larger extent among sites.

Study of water stable isotope composition in frozen ground was shown to provide additional useful information to reconstruct past hydrology supporting the results from other paleo-environmental proxies. Variations in the isotopic ratio profiles are found to be useful to know the past dynamics of floodplain development. For example, not all but some profiles of $\delta^{18}O$ values showed certain change in the values continuity or range of variation at the depths which were likely to be recent maximum thaw depth or permafrost table (e.g., B2, B3, B4, K2, VK4, or F2). Thawing of seasonally frozen soils in spring makes water in the active layer mobile and allows exchange with meteoric water inputs in the later period; therefore, it could be expected that certain unconformity in water stable isotope ratio exists around the depth of recent maximum thaw. Maximum thaw depth in each year can largely vary due to changing meteorological conditions as shown in Fig. 4 even when landscape remains the same, so this information from stable isotope could provide a memory of the past extreme thaw event. Furthermore, the $\delta^{18}O$ values between −20 and −25‰ and the d-excess values around 10‰ in the upper 1 m horizons are common features in ground ice stable isotopes on relatively high topography among the study sites. In addition, overall trend of the $\delta^{18}O$ values change in the upper 1 m decreased with depth. Those similarities suggest that a common hydrological process have been occurring during formation of upper 1 m soil profiles in our research area.

The uppermost layer, which is subject to episodic thaw at sub-decadal to multi-centennial scales, is known as the transition zone (Shur et al., 2005; French and Shur, 2010). This upper permafrost zone between the active layer and lower permafrost often has high ice content because this ground layer experiences favorable thermal and hydrological conditions for ice segregation (slow freezing rate and water saturation). The transition zone is important for permafrost stability and serves as a buffer between the active layer and ice-rich permafrost, especially permafrost containing massive ice (Shur et al., 2005). Our results showed the possibility for using profiles of water stable isotopes to identify or determine the transition zone, together with dating of the soil layers. In order to obtain the indication of change in isotopic values, however, isotopic discrimination upon permafrost

Table 2
Summary of statistics for $\delta^{18}O$, δD, and d-excess of river, wedge ice (WI), and soil water. Sample depth was divided into upper (0–0.5 m depth) and lower layers approximately designated as active layer (AL) and permafrost (PF), respectively. The wedge ice samples were taken only from lower than 1.0 m depth. *N*, Min, Ave, Max, and Sd indicate number of samples, minimum, average, maximum, and standard deviation, respectively.

Site/Sample type	*N*	Depth (m)	$\delta^{18}O$ (‰)				δD (‰)				D-excess (‰)			
			Min	Ave	Max	Sd	Min	Ave	Max	Sd	Min	Ave	Max	Sd
B	10	AL (0–0.5)	−23.4	−21.6	−19.7	1.2	−171	−160	−147	8	10.6	13.2	18.9	2.7
	34	PF (>0.5)	−25.4	−22.7	−19.1	1.6	−196	−175	−157	11	−7.4	6.6	14.6	4.4
	13	WI (B3)	−29.6	−28.3	−26.8	1.0	−224	−215	−204	6	6.4	11.8	15.9	2.5
K	8	AL (0–0.5)	−22.9	−21.9	−20.4	0.9	−175	−166	−156	7	7.2	9.6	11.5	1.8
	32	PF (>0.5)	−24.7	−23.0	−18.4	1.3	−189	−178	−154	8	−6.6	5.8	11.9	3.8
	8	WI (K2)	−26.7	−26.1	−25.6	0.4	−204	−201	−198	3	5.0	7.3	9.8	1.7
VK	16	AL (0–0.5)	−22.2	−20.8	−19.2	0.9	−167	−158	−147	5	0.6	8.3	13.3	3.8
	53	PF (>0.5)	−23.9	−21.5	−16.7	1.5	−187	−169	−152	8	−19.9	2.7	12.2	6.8
F	3	AL (0–0.5)	−18.9	−18.6	−18.3	0.3	−156	−154	−152	2	−5.5	−5.0	−4.5	0.5
	17	PF (>0.5)	−23.0	−20.5	−18.2	1.7	−181	−169	−153	9	−22.4	−5.4	6.3	9.8
A	–	AL (0–0.5)	–	–	–	–	–	–	–	–	–	–	–	–
	8	PF (>0.5)	−23.9	−22.5	−21.2	0.8	−178	−167	−157	7	12.8	13.6	14.4	0.6
River water	20		−21.4	−20.7	−19.9	0.4	−164	−162	−155	2	2.2	4.5	7.3	1.3

aggradation (O'Neil, 1968; Suzuoki and Kimura, 1973) must be taken into account for the interpretations.

Water stable isotope composition also includes information of source of the ground ice and how the ice water had been evaporatively-enriched. Determining the origin of B2 profile ice is difficult because we could obtain a limited number of water samples from the Indigirka River during July of 2009 and 2010, and no rain samples are available. However, Welp et al. (2005) reported seasonal variation (September 2002–April 2004) in $\delta^{18}O$ values of the Kolyma River water at Cherskii, about 550 km east of Chokurdakh. The water of the Kolyma River showed values around −22‰ except spring snow melt season with negative peak value of −24.4‰ on 7 June 2003. The negative peak values quickly recovered to the average range before July. Assuming this seasonal change in $\delta^{18}O$ values is also similar to that of the Indigirka River, the water samples we obtained from the river were thought to be those after snow melt runoff, and the $\delta^{18}O$ values were around −21‰ (Table 2). These values partly match the values at B2, and other values with lower d-excess values (Figs. 7 and 14) could be treated as surface water kinetically enriched by evaporation, and those might be along a local meteoric water line. Similar distribution of water stable isotope ratio of surface water (wetland and lakes) on co-isotope plot for Canadian Arctic has reported by St Amour et al. (2005). Rain water as an origin of the B2 ground ice is less likely because stable isotope ratio of rain in the Arctic regions of northeastern Siberia were reported to have heavier range and to be less evaporatively-enriched (e.g. Schwamborn et al., 2008; Meyer et al., 2000, 2002; Opel et al., 2011). Consequently, development of the ground ice at site B can be speculated as following. At least upper 1.5 m of the ice-rich deposit was formed syngenetically with floods of unknown frequency, and relatively low center areas of low-centered polygons preferentially had kept flood water subsequently incorporated into permafrost, while higher areas such as polygon rims could keep much less flood water and most composition of the water could be summer precipitation. On the other hand, frost cracks formed on polygonal networks during winter had been filled by snow melt water and refreeze before flooding seasons. There is another possibility that B2 was a part of former frost crack free from filling by snowmelt water by some reason, and flood water has filled the cavity around B2 location making B2 ice distinct from others. More evidences from sediments' dating and stable isotope analysis with spatially denser samplings are necessary for further discussion.

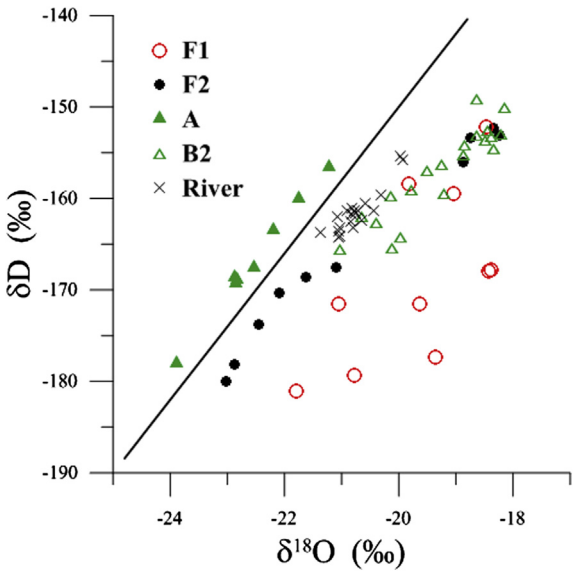

Fig. 14. Co-isotope relationship of the Indigirka River, ground water/ice at F1, F2, A, and B2 points.

5. Conclusions

The diversity in geocryological characteristics of frozen ground including ice content, cryostratigraphy, soil mechanical characteristics, organic content and components, and water stable isotope ratio can provide valuable information to reconstruction of terrestrial paleo-environment in permafrost regions. These data contain important information about the surface environment during the permafrost formation. Information from stable isotopes in frozen ground could provide a memory of the past extreme thaw event, as thawing of seasonally frozen soils in spring makes water in the active layer mobile and allows exchange with meteoric water inputs in the later period. The $\delta^{18}O$ values between −20 and −25‰ and the d-excess values around 10‰ in the upper 1 m horizons are common features in ground ice stable isotopes at dry areas (relatively higher topography) among the study sites. In addition, overall trend of the $\delta^{18}O$ values change in the upper 1 m decreased with depth. The d-excess values in the lower active layer (0.5–0.7 m depth) at wet areas were remarkably lower than those at dry areas. This lower d-excess may be explained by site-specific micro-reliefs, which determine the areas that preferably collect meteoric water (relatively lower wet areas) and maintain water ponding, exposing water to evaporation during summer. Regarding to cryostratigraphy, more developed cryostructure with thicker ice lenses or veins

tended to be found at higher and dry areas than at lower wet areas. From these similarities in geocryological characteristics or relationship between each characteristic between study sites, it is suggested here that similar hydrological conditions have influenced formation of upper 1-m cryostratigraphy in our research area. These kinds of geocryological analyses appear to be strong tool for understanding development history of sedimentation and permafrost aggradation, and influence of flooding on permafrost degradation/aggradation in floodplains in permafrost regions. In addition, information regarding permafrost development (flood history, ice wedge formation, thawing events, etc.) in the past can be inferred from the spatial distribution of geocryological properties of the near-surface ground.

Acknowledgments

This work was supported by Grant-in-Aids, the Global COE Program "Establishment of Center for Integrated Field Environmental Science" (IFES-GCOE) from the Ministry of Education, Culture, Sports, Science and Technology (MEXT), the JSPS Institutional Program for Young Researcher Overseas Visits, and the JSPS KAKENHI Grant Number, and the IARC – JAXA Information System (IJIS) with funding provided by the Japan Aerospace Exploration Agency (JAXA) under a grant to the International Arctic Research Center (IARC). We wish to thank rangers of Chokurdakh Nature Protection and researchers and engineers in the Institute for Biological Problems of Cryolithozone for their help during fieldwork. Isotopic analyses were conducted under the support of Dr. Ueta, Ms. Hoshino, and Ms. Ohnishi.

References

Arkhangelov, A.A., Baykmyae, R.A., Mikhalev, D.V., Punning, Y.-M.K., Solomatin, V.I., 1986. Stratigraphic subdivision of syngenetic permafrost by means of oxygen-isotope analysis. Trans. (Doklady) USSR Acad. Sci. Earth Sci. Sect. 290 (2), 94–96.

Bagard, M.-L., Chabaux, F., Pokrovsky, O.S., Viers, J., Prokushkin, A.S., Stille, P., Rihs, S., Schmitt, A.-D., Dupre, B., 2011. Seasonal variability of element fluxes in two Central Siberian rivers draining high latitude permafrost dominated areas. Geochim. Cosmochim. Acta 75 (12), 3335–3357.

Beskow, G., 1935. Soil Freezing and Frost Heaving with Special Application to Roads and Railroads. The Swedish Geological Society, C, no. 375, Year Book no. 3. Technological Institute, Northwestern University.

Brosius, L.S., Anthony, K.M.W., Grosse, G., Chanton, J.P., Farquharson, L.M., Overduin, P.P., Meyer, H., 2012. Using the deuterium isotope composition of permafrost meltwater to constrain thermokarst lake contributions to atmospheric CH_4 during the last deglaciation. J. Geophys. Res. Biogeosci. 117.

Brutsaert, W., Hiyama, T., 2012. The determination of permafrost thawing trends from long-term streamflow measurements with an application in Eastern Siberia. J. Geophys. Res. Atmos. 117, D22110.

Casagrande, A., 1932. A new theory of frost heaving: discussion. Proc. Annu. Meet. Highway Res. Board 11 (1), 168–172.

Dansgaard, W., 1964. Stable isotopes in precipitation. Tellus 16 (4), 436–468.

Department of Geodesy and Cartography, USSR, 1989. Agricultural Atlas of Yakutskaya Autonomous Soviet Socialist Republic (in Russian).

Department of Geodesy and Cartography, USSR, 1991. Permafrost-landscape Map of Yakutskaya Autonomous Soviet Socialist Republic (in Russian).

Ershov, E.D. (Ed.), 1989. Geocryology of USSR, Eastern Siberia and Far East. Nedra, Moscow, p. 515 (in Russian).

Everdingen, R.V. (Ed.), 1998. Multi-language Glossary of Permafrost and Related Ground-ice Terms, Boulder. National Snow and Ice Data Center/World Data Center for Glaciology, CO, p. 88 (revised January 2002).

Francis, J.A., White, D.M., Cassano, J.J., Gutowski Jr., W.J., Hinzman, L.D., Holland, M.M., Steele, M.A., Voeroesmarty, C.J., 2009. An arctic hydrologic system in transition: feedbacks and impacts on terrestrial, marine, and human life. J. Geophys. Res. Biogeosci. 114, G04019.

French, H., Shur, Y., 2010. The principles of cryostratigraphy. Earth-Sci. Rev. 101 (3–4), 190–206.

Grave, N.A., Turbina, M.I. (Eds.), 1980. Stability of Near-surface Ground to Anthropogenic Impacts in Permafrost Regions. Permafrost Institute, Yakutsk, Russia, p. 142 (in Russian).

Grosse, G., Romanovsky, V., Jorgenson, T., Anthony, K.W., Brown, J., Overduin, P.P., 2011. Vulnerability and feedbacks of permafrost to climate change. Eos Trans. AGU 92 (9), 73–74.

Haeberli, W., Burn, C.R., 2002. Natural Hazards in Forests: Glacier and Permafrost Effects as Related to Climate Change. CABI Publishing, Wallingford, New York.

Heiri, O., Lotter, A.F., Lemcke, G., 2001. Loss on ignition as a method for estimating organic and carbonate content in sediments: reproducibility and comparability of results. J. Paleolimnol. 25 (1), 101–110.

IPCC, 2007. Summary for policymakers. In: Solomon, S., Qin, D., Manning, M., Chen, Z., Marquis, M., Al, E. (Eds.), Climate change 2007: the physical science basis. Working Group I Contribution to the Fourth Assessment Report of the Intergovernmental Panel on Climate Change. Cambridge University Press, Cambridge, United Kingdom and New York, NY, USA.

Jorgenson, M.T., Romanovsky, V., Harden, J., Shur, Y., O'donnell, J., Schuur, E.a.G., Kanevskiy, M., Marchenko, S., 2010. Resilience and vulnerability of permafrost to climate change. Can. J. For. Research Rev. 40 (7), 1219–1236.

Kachinsky, N.A., 1958. Mechanical and Microagregate Composition of Soils, Methods of Analysis. Moscow Academy of Sciences, Moscow, p. 192 (in Russian).

Kanevskiy, M., Shur, Y., Fortier, D., Jorgenson, M.T., Stephani, E., 2011. Cryostratigraphy of late Pleistocene syngenetic permafrost (yedoma) in northern Alaska, Itkillik River exposure. Quat. Res. 75 (3), 584–596.

Kanevskiy, M., Shur, Y., Jorgenson, M.T., Ping, C.L., Michaelson, G.J., Fortier, D., Stephani, E., Dillon, M., Tumskoy, V., 2013. Ground ice in the upper permafrost of the Beaufort Sea coast of Alaska. Cold Regions Sci. Technol. 85, 56–70.

Koven, C.D., Ringeval, B., Friedlingstein, P., Ciais, P., Cadule, P., Khvorostyanov, D., Krinner, G., Tarnocai, C., 2011. Permafrost carbon-climate feedbacks accelerate global warming. Proc. Natl. Acad. Sci. U.S.A. 108 (36), 14769−14774.

Kuznetsova, T., 1980. Engineering-geocryological conditions and stability of permafrost in maritime lowland of Yakutia to disturbance of natural environment. In: Grave, N.A., Turbina, M.I. (Eds.), Stability of Near-surface Ground to Anthropogenic Impacts in Permafrost Regions. Permafrost Institute, Yakutsk, Russia, pp. 75−107 (in Russian).

Lawrence, D.M., Slater, A.G., Tomas, R.A., Holland, M.M., Deser, C., 2008. Accelerated Arctic land warming and permafrost degradation during rapid sea ice loss. Geophys. Res. Lett. 35 (11), L11506.

Lawrence, D.M., Slater, A.G., Swenson, S.C., 2012. Simulation of present-day and future permafrost and seasonally frozen ground conditions in CCSM4. J. Clim. 25 (7), 2207−2225.

Mackay, J.R., 1983. Oxygen isotope variations in permafrost, Tuktoyaktk Peninsula area, Northwest Territories. Pap. Geol. Surv. Can. B. 18, 67−74.

Merlivat, L., Jouzel, J., 1979. Global climatic interpretation of the deuterium-oxygen 18 relationship for precipitation. J. Geophys. Res. 84 (C8), 5029−5033.

Meyer, H., Dereviagin, A.Y., Siegert, C., Hubberten, H.W., 2000. Paleoclimate studies on Bykovsky Peninsula, north Siberia − hydrogen and oxygen isotopes in ground ice. Polarforschung 70, 37−51.

Meyer, H., Dereviagin, A., Siegert, C., Schirrmeister, L., Hubberten, H.W., 2002. Palaeoclimate reconstruction on Big Lyakhovsky Island, north Siberia − hydrogen and oxygen isotopes in ice wedges. Permafrost Periglacial Process. 13 (2), 91−105.

Meyer, H., Schirrmeister, L., Andreev, A., Wagner, D., Hubberten, H.-W., Yoshikawa, K., Bobrov, A., Wetterich, S., Opel, T., Kandiano, E., Brown, J., 2010. Lateglacial and holocene isotopic and environmental history of northern coastal Alaska − results from a buried ice-wedge system at Barrow. Quat. Sci. Rev. 29 (27−28), 3720−3735.

Michel, F.A., 2011. Isotope characterization of ground ice in Northern Canada. Permafrost Periglacial Process. 22 (1), 3−12.

Morse, P.D., Burn, C.R., Kokelj, S.V., 2009. Near-surface ground-ice distribution, Kendall island bird sanctuary, western Arctic coast, Canada. Permafrost Periglacial Process. 20 (2), 155−171.

Murton, J.B., French, H.M., 1994. Cryostructures in permafrost, Tuktoyaktuk coastlands, western Arctic Canada. Can. J. Earth Sci. 31 (4), 737−747.

O'Neil, J.R., 1968. Hydrogen and oxygen isotope fractionation between ice and water. J. Phys. Chem. 72, 3683−3684.

Opel, T., Dereviagin, A.Y., Meyer, H., Schirrmeister, L., Wetterich, S., 2011. Palaeoclimatic information from stable water isotopes of Holocene ice wedges on the Dmitrii Laptev Strait, Northeast Siberia, Russia. Permafrost Periglacial Process. 22 (1), 84−100.

Osterkamp, T.E., 2005. The recent warming of permafrost in Alaska. Glob. Planet. Change 49 (3−4), 187−202.

Outcalt, S.I., Nelson, F.E., Hinkel, K.M., 1990. The zero-curtain effect: heat and mass transfer across an isothermal region in freezing soil. Water Resour. Res. 26 (7), 1509−1516.

Palmer, M.J., Burn, C.R., Kokelj, S.V., 2012. Factors influencing permafrost temperatures across tree line in the uplands east of the Mackenzie Delta, 2004−2010. Can. J. Earth Sci. 49 (8), 877−894.

Ping, C.-L., Michaelson, G.J., Guo, L., Jorgenson, M.T., Kanevskiy, M., Shur, Y., Dou, F., Liang, J., 2011. Soil carbon and material fluxes across the eroding Alaska Beaufort Sea coastline. J. Geophys. Res. Biogeosci. 116.

Pullman, E.R., Jorgenson, M.T., Shur, Y., 2007. Thaw settlement in soils of the Arctic coastal plain, Alaska. Arctic Antarctic Alpine Res. 39 (3), 468−476.

Romanovsky, V.E., Sazonova, T.S., Balobaev, V.T., Shender, N.I., Sergueev, D.O., 2007. Past and recent changes in air and permafrost temperatures in Eastern Siberia. Glob. Planet. Change 56 (3−4), 399−413.

Romanovsky, V.E., Drozdov, D.S., Oberman, N.G., Malkova, G.V., Kholodov, A.L., Marchenko, S.S., Moskalenko, N.G., Sergeev, D.O., Ukraintseva, N.G., Abramov, A.A., Gilichinsky, D.A., Vasiliev, A.A., 2010. Thermal state of permafrost in Russia. Permafrost Periglacial Process. 21 (2), 136−155.

Rowland, J.C., Jones, C.E., Altmann, G., Bryan, R., Crosby, B.T., Hinzman, L.D., Kane, D.L., Lawrence, D.M., Mancino, A., Marsh, P., Mcnamara, J.P., Romanvosky, V.E., Toniolo, H., Travis, B.J., Trochim, E., Wilson, C.J., Geernaert, G.L., 2010. Arctic landscapes in transition: responses to thawing permafrost. Eos Trans. AGU 91 (26), 229−230.

Schirrmeister, L., Kunitsky, V., Grosse, G., Wetterich, S., Meyer, H., Schwamborn, G., Babiy, O., Derevyagin, A., Siegert, C., 2011. Sedimentary characteristics and origin of the Late Pleistocene ice complex on north-east Siberian Arctic coastal lowlands and islands − a review. Quat. Int. 241, 3−25.

Schirrmeister, L., Froese, D., Tumskoy, V., Grosse, G., Wetterich, S., 2013. Yedoma: Late Pleistocene ice-rich syngenetic permafrost of Beringia. In: Elias, S.A. (Ed.), Encyclopedia of Quaternary Science, second ed. Elsevier, pp. 542−552.

Schuur, E.a.G., Bockheim, J., Canadell, J.G., Euskirchen, E., Field, C.B., Goryachkin, S.V., Hagemann, S., Kuhry, P., Lafleur, P.M., Lee, H., Mazhitova, G., Nelson, F.E., Rinke, A., Romanovsky, V.E., Shiklomanov, N., Tarnocai, C., Venevsky, S., Vogel, J.G., Zimov, S.A., 2008. Vulnerability of permafrost carbon to climate change: implications for the global carbon cycle. Bioscience 58 (8), 701−714.

Schwamborn, G., Fedorov, G., Schirrmeister, L., Meyer, H., Hubberten, H.-W., 2008. Periglacial sediment variations controlled by late quaternary climate and lake level change at Elgygytgyn crater, Arctic Siberia. Boreas 37 (1), 55−65.

Shiklomanov, A.I., Lammers, R.B., 2009. Record Russian river discharge in 2007 and the limits of analysis. Environ. Res. Lett. 4 (4), 045015.

Shur, Y., Hinkel, K.M., Nelson, F.E., 2005. The transient layer: implication for geocryology and climate-change science. Permafrost Periglacial Process. 16, 5−17.

Sjoberg, Y., Frampton, A., Lyon, S.W., 2013. Using streamflow characteristics to explore permafrost thawing in northern Swedish catchments. Hydrogeol. J. 21 (1), 121−131.

Smith, S.L., Throop, J., Lewkowicz, A.G., 2012. Recent changes in climate and permafrost temperatures at forested and polar desert sites in northern Canada. Can. J. Earth Sci. 49 (8), 914−924.

St Amour, N.A., Gibson, J.J., Edwards, T.W.D., Prowse, T.D., Pietroniro, A., 2005. Isotopic time-series partitioning of streamflow components in wetland-dominated catchments, lower Liard River basin, northwest territories, Canada. Hydrol. Process. 19 (17), 3357−3381.

Strauss, J., Schirrmeister, L., Wetterich, S., Borchers, A., Davydov, S.P., 2012. Grain-size properties and organic-carbon stock of yedoma ice complex permafrost from the Kolyma

lowland, northeastern Siberia. Glob. Biogeochem. Cycle 26, GB004104.

Suzuoki, T., Kimura, T., 1973. D/H and $^{18}O/^{16}O$ fractionation in ice-water system. Mass Spectrosc. 21 (3), 229−233.

Takashi, T., Masuda, M., Yamamoto, H., 1974. Experimental study on the influence of freezing speed upon frost heave ratio of soil under constant effective stress. Seppyo 36 (2), 49−68 (in Japanese with English abstract).

Ueta, A., Sugimoto, A., Iijima, Y., Yabuki, H., Maximov, T.C., Velivetskaya, T.A., Ignatiev, A.V., 2013. Factors controlling diurnal variation in the isotopic composition of atmospheric water vapour observed in the taiga, Eastern Siberia. Hydrol. Process. 27 (16), 2295−2305.

Vaikmae, R., 1989. Oxygen Isotopes in Permafrost and in Ground Ice − a New Tool for Paleoclimatic Investigations. Paper presented at 5th Working Meeting Isotopes in Nature, Leipzig, September.

Van Der Molen, M.K., Van Huissteden, J., Parmentier, F.J.W., Petrescu, A.M.R., Dolman, A.J., Maximov, T.C., Kononov, A.V., Karsanaev, S.V., Suzdalov, D.A., 2007. The growing season greenhouse gas balance of a continental tundra site in the Indigirka Lowlands, NE Siberia. Biogeosciences 4 (6), 985−1003.

Van Huissteden, J., Maximov, T.C., Dolman, A.J., 2005. High methane flux from an arctic floodplain (Indigirka Lowlands, Eastern Siberia). J. Geophys. Res. Biogeosci. 110 (G2).

Walter, K.M., Zimov, S.A., Chanton, J.P., Verbyla, D.,F.S., Chapin, I., 2006. Methane bubbling from Siberian thaw lakes as a positive feedback to climate warming. Nature 443 (7107), 71−75.

Welp, L.R., Randerson, J.T., Finlay, J.C., Davydov, S.P., Zimova, G.M., Davydova, A.I., Zimov, S.A., 2005. A high-resolution time series of oxygen isotopes from the Kolyma River: implications for the seasonal dynamics of discharge and basin-scale water use. Geophys. Res. Lett. 32 (14).

Zaitsev, V.N., 1989. Chapter 12. Yana-Kolyma region, natural conditions. In: Ershov, E.D. (Ed.), Geocryology of USSR, Eastern Siberia and Far East. Nedra, Moscow, pp. 240−249 (in Russian).

Zimov, S.A., Voropaev, Y.V., Semiletov, I.P., Davidov, S.P., Prosiannikov, S.F., Iii, F.S.C., Chapin, M.C., Trumbore, S., Tyler, S., 1997. North Siberian lakes: a methane source fueled by Pleistocene. Science 277 (5327), 800−802.